UDK 669.715:620.187:544.015.4
Original scientific article/Izvirni znanstveni članek

ISSN 1580-2949
MTAEC9, 46(6)563(2012)

INFLUENCE OF THE COOLING RATE ON THE MICROSTRUCTURE DEVELOPMENT OF THE EN AW-AlMg4.5Mn0.7 ALLOY

VPLIV OHLAJEVALNE HITROSTI NA RAZVOJ MIKROSTRUKTURE V ZLITINI EN AW-AlMg4,5Mn0,7

Natalija Dolić[1], Jožef Medved[2], Primož Mrvar[2], Faruk Unkić[1]

[1]University of Zagreb, Faculty of Metallurgy, Aleja narodnih heroja 3, 44103 Sisak, Croatia
[2]University of Ljubljana, Faculty of Natural Sciences and Engineering, Department of Materials and Metallurgy, Aškerčeva c. 12, 1000 Ljubljana, Slovenia
ndolic@simet.hr

Prejem rokopisa – received: 2012-03-01; sprejem za objavo – accepted for publication: 2012-04-05

In this work, the course of the solidification and development of the microstructure of a sample of the EN AW-AlMg4.5Mn0.7 alloy, taken out from the edge of a slab cast with a semi-continuous, vertical, direct water-cooling process (DC) was studied.
In order to determine the influence of the cooling rate on the type, the morphology and the solidification course of some phases in EN AW-AlMg4.5Mn0.7, a simultaneous thermal analysis using differential scanning calorimetry was conducted. Its results were compared with the thermodynamically calculated equilibrium phases obtained on the basis of the Thermo-Calc software. The results were also compared with the results of a simple thermal analysis, which was conducted by casting the sample in a specially designed measuring cell using the Croning process and in a cone-shaped measuring cell. The temperature intervals of the reference temperature-phase transitions (the liquidus temperature T_L, the temperature evaluation of the first eutectic T_{E1} and the second eutectic T_{E2} and the solidus temperature T_S) and the times of the solidification Δt_s of the EN AW-AlMg4.5Mn0.7 alloy were determined. The mathematical models describing the changes in these parameters depending on the cooling rate were made.
Using a quantitative analysis carried out with an energy dispersive spectrometer, the following microstructural constituents were determined: the intermetallic phase $Al_6(Fe, Mn)$, which, due to an unequilibrium evaluation, corresponds to the first eutectic (α_{Al} + $Al_6(Fe, Mn)$ and the Mg_2Si intermetallic phase, as the second eutectic phase (α_{Al} + Mg_2Si). In addition, the presence of the pores was determined. The total surface area of some intermetallic phases and pores and their distribution in dependence on the cooling rate were examined by a scanning electron microscope.

Keywords: EN AW-AlMg4.5Mn0.7 alloy, cooling rate, microstructure

V delu obravnavamo potek strjevanja in razvoj mikrostrukture zlitine EN AW-AlMg4,5Mn0,7. Vzorec je bil odvzet na robu slaba, ulitega po polkontinuirnem postopku z direktnim vodnim hlajenjem v navpični smeri ("DC").
Za opredelitev vpliva ohlajevalne hitrosti na potek strjevanja v zlitini EN AW-AlMg4,5Mn0,7 in s tem na razvoj faz je bila uporabljena simultana termična analiza z diferenčno vrstično kalorimetrijo. Dobljene rezultate smo primerjali s termodinamsko ravnotežnimi izračuni posameznih faz. Izračun je bil narejen s programom "Thermo-Calc". Primerjava je bila narejena tudi z rezultati, dobljenimi z enostavno termično analizo. V tem primeru smo vzorec ulili v merilno celico, narejeno po postopku Cronning, in v trajno kokilo stožčaste oblike. Tako smo določili karakteristične temperature faznih transformacij (temperaturo liquidusa T_L, temperaturo prvega T_{E1} in drugega evtektika T_{E2} ter temperaturo solidusa T_S) ter čase strjevanja zlitine Δt_s. Za opis teh, od hitrosti odvisnih parametrov, smo izdelali tudi matematični model.
Kvantitativna analiza posameznih faz oziroma identifikacija le-teh je bila narejena z energijsko-disperzijsko spektroskopijo rentgenskih žarkov. Opredeljene so bile naslednje mikrostrukturne sestavine: intermetalna faza $Al_6(Fe, Mn)$, ki je v zvezi z neravnotežnim strjevanjem prvega evtektika (α_{Al} + $Al_6(Fe, Mn)$), intermetalno fazo Mg_2Si, ki je del evtektskega heterogenega zloga (α_{Al} + Mg_2Si). Prav tako smo naredili analizo poroznosti. Za opredelitev deleža poroznosti, kot tudi posameznih intermetalnih faz in njihovo porazdelitev v odvisnosti od ohlajevalne hitrosti, je bil uporabljen vrstični elektronski mikroskop.

Ključne besede: zlitina EN AW-AlMg4,5Mn0,7, ohlajevalna hitrost, mikrostruktura

1 INTRODUCTION

Aluminum and its alloys are used in a variety of applications in industry and construction. Typical applications of aluminum alloys are found in the automotive industry, in the maritime, air and railway transportations. Recently, aluminum has been competing with steel in the automotive industry for the production of engine parts, suspensions and car-space frames. In most of these applications rolled products are used with a thickness of 0.1–25 mm.[1] Intensive industrial competition requires a continuous quality improvement. The main motivation for this activity originates in the growing demands of the industry for a development of high-strength alloys in order to reduce the weight of various products.[1]

Aluminum-magnesium alloys constitute a group of non-heat treatable alloys with a medium strength, high ductility, an excellent corrosion resistance and weldability (the 5XXX series). Wrought Al-Mg alloys are used as structural materials for marine, automotive, aircraft and cryogenic applications, while their cast forms are mainly used, due to the corrosion resistance, in dairy, food-handling and chemical-processing applications.[2–4] The EN AW-AlMg4.5Mn0.7 alloy is one of the most popular commercial alloys that is mostly used for ship

structures due to its superior resistance against corrosion.[5]

The non-heat treatable aluminum alloys are utilized in all of the major industrial markets for aluminum flat-rolled products. At the end of the 20th century, transportation, packaging and building/construction sectors represented the largest users of the non-heat-treatable sheets. High-performance, non-heat-treatable alloys were developed for the new and existing applications ranging from foil to high-strength structural products. The development of the new or improved alloys was based on the need for a structural performance or appearance in the end products and the productivity during the customer's manufacturing process.[1]

The polythermal section of the ternary Al-Mg-Mn phase diagram shown in **Figure 1** gives us the first approximation of the phase-transformation history for the alloys like EN AW-5083, EN AW-5182, and EN AW-5456 containing the mass fraction of Mg 4.0–7.0 % and 0.3–0.6 % Mn. The solidification starts at 635–640 °C with the formation of the α_{Al} grains. After that, providing that the concentration of Mn is sufficient, the (α_{Al} + Al_6Mn) eutectics are formed in the temperature range from 627 °C to 617 °C. These reactions seldom occur during the cooling following the solidification because, due to a relatively low diffusion coefficient, manganese usually remains in the supersaturated solid solution.[6]

The presence of silicon, as an impurity or an alloying element, in the Al-Mg-Mn alloys results in the formation of Mg_2Si in addition to other phases. Most commercial alloys contain iron as an impurity. As a result, the (α_{Al} + Al_6(Fe, Mn)) eutectics are formed in the temperature range from 600 °C to 570 °C, and the solidification is completed at approximately 570 °C with the formation of the (α_{Al} + Al_6(Fe, Mn) + Al_3Fe) eutectics. Under equilibrium, the other phases that are frequently observed in the Al-Mg-Mn-Fe alloys, e.g., Al_8Mg_5 (previously known as Al_3Mg_2[7–9]) and Al_{10}(Mg, Mn)$_3$, are formed only due to the precipitation from the aluminum solid solution upon cooling in the solid state. Under the real, non-equilibrium conditions, these phases can be formed during the solidification being a result of the eutectic reaction.[6] In the case of a simultaneous presence of iron and silicon in a 5XXX series alloy containing 5 % Mg (e.g., the EN AW-5182 alloy), the solidification will end at 576–578 °C with the formation of Mg_2Si by a eutectic reaction.[6]

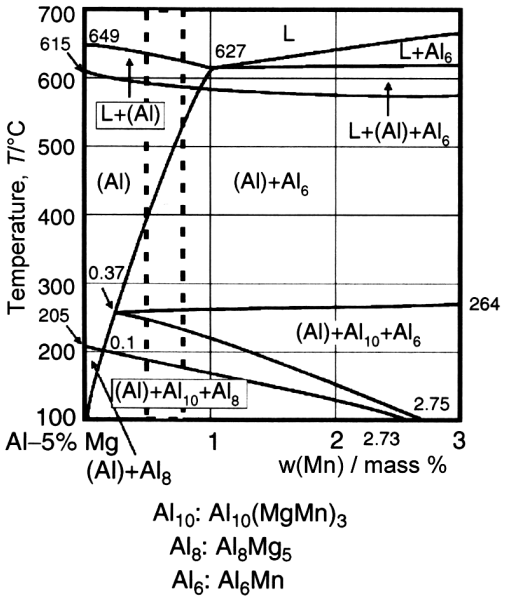

Figure 1: Isopleths of the Al-Mg-Mn phase diagram at the mass fraction of Mg 5 % [6]

Slika 1: Ravnotežni izopletni fazni diagram Al-Mg-Mn pri masnem deležu Mg 5 % [6]

The solidification paths that we considered above, describe the phase equilibrium and can hardly be accomplished under the real casting conditions when the cooling rates are high and the diffusion processes, especially in the solid phase, cannot be completed to such an extent that the compositions of the phases change with the temperature in accordance with the equilibrium-phase diagram. Local deviations from equilibrium result in a microsegregation and, eventually, in the shift of local equilibrium to the concentrations, where new phases are formed. In addition, some high-temperature peritectic reactions remain uncompleted and the high-temperature phases – that have to disappear as a result of these reactions – are retained at a lower temperature and can be found in the solid state.[6]

For all aluminum-alloy components, the casting process plays an important role in controlling the properties of the final products. Semi-continuous Direct Chill (DC) casting is the most common method used for producing aluminum-alloy ingots for the subsequent thermomechanical processing (TMP), such as rolling and extrusion.[10,11] Casting defects such as microsegregation and porosity are usually present in the as-cast microstructure and can lead to a deterioration of mechanical properties. Many studies have shown a detrimental effect of porosity on the fatigue properties of the materials used in the as-cast or heat-treated state.[11,12]

2 EXPERIMENTAL WORK

Tests were carried out on a sample of an ingot cast by semi-continuous, vertical, direct water-cooling process (Direct Chill), having the dimensions of 520 mm × 1 680 mm × 4 809 mm and being produced from charge 3116 of the EN AW-AlMg4.5Mn0.7 alloy (the numerical symbol EN AW-5083).[13] The structure of the tested alloy 3116 contains a significantly higher share of the technological waste, compared to the primary aluminum, in the ratio of 75 : 25. The main components of the technological waste are the alloys EN AW-1050, EN AW-5049 and EN AW-5754. Before casting, the melt

was refined with a mixture of argon and chlorine in an ALPUR unit. The grain refinement was performed by adding the AlTi5B master alloy in the form of small bars (in the melting furnace) and wires (into the groove in front of ALPUR), in an average quantity of 1.74 kg/t of the melt.[14]

From the ingot cast in this way, an about 30-mm thick, transversally cut plate was taken out from its front part, after having been disposed of the technological waste of about 200 mm at the beginning of the casting. From the cut plate, from its edge, a part of the ingot was taken out and used to perform tests with a simple thermal analysis (STA) and differential scanning calorimetry (DSC).

The thermodynamical calculation of the phase equilibrium of the EN AW-AlMg4.5Mn0.7 charge-3116 alloy was preliminary performed by the Thermo-Calc (TCW 5.0) software. This software allows a calculation of the phase stability of particular phases taking into account the equilibrium conditions of temperature, pressure and chemical composition.

The simple thermal analysis was performed on sample 6P-1 (in the as-cast condition) taken out from the beginning of the cast ingot of charge 3116. Sample 6P-1 was molten in the graphite pot of an electric furnace. When the melt reached the temperature of approximately 730 °C, it was poured from the graphite pot into two measuring cells: into a cell made with the Croning process (equipped with a single thermocouple in the middle), **Figure 2a**, and a permanent cone-shaped measuring cell (**Figure 2b**). For the characterization of the solidification of sample 6P-1 at different cooling rates, the cone-shaped measuring cell of grey cast iron was used with three thermocouples installed in it. The described measuring cells are illustrated in **Figures 2a** and **2b**.

The samples for the metallographic and microstructural investigations were taken out from the corresponding place in the immediate neighborhood of the thermocouple. These samples are illustrated in **Figures 3a** and **3b**.

The samples for the metallographic and microstructural investigation were prepared with a standard procedure of grinding and polishing, and afterwards etching in 0.5 % HF. The samples for the microstructural investigation were examined on a scanning electron microscope (SEM) TESCAN VEGA TS5136LS with phase recognition performed on the basis of a chemical-composition analysis made with the energy dispersive spectrometer (EDS).

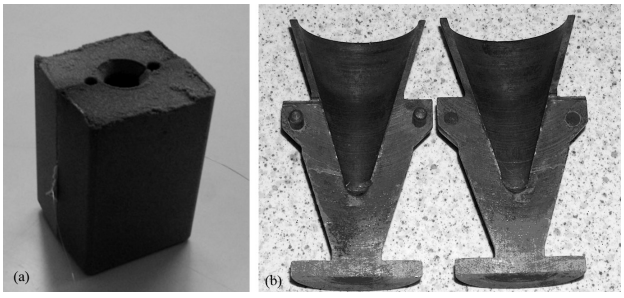

Figure 2: Measuring cell made: a) with the Croning process and b) the cone-shaped grey iron-measuring cell

Slika 2: Merilna celica, narejena: a) po postopku Croning in b) stožčasta merilna celica iz sive litine

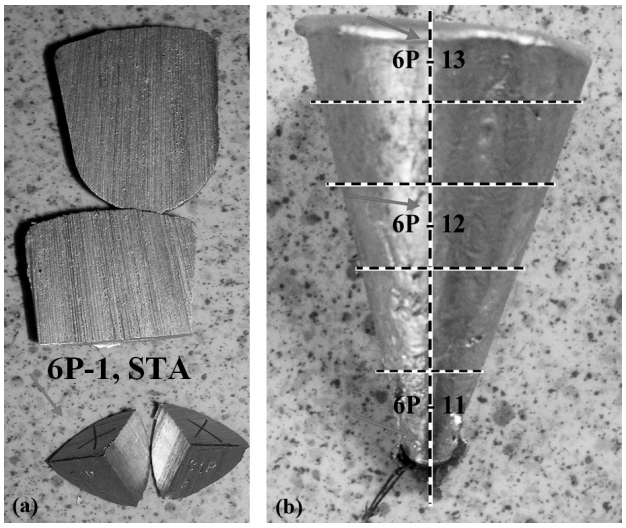

Figure 3: Sampling methodology for the metallographic and microstructural analysis with the marked places of the performed analysis: a) photography of a cut sample poured into the measuring cell made with the Croning process with a marked place of sample taking and a description; b) photography of a cut sample poured into the permanent cone-shaped measuring cell with the marked places of sample taking and a description

Slika 3: Prikaz mesta odvzema vzorcev v ulitku za metalografsko in mikrostrukturno analizo s pripadajočimi oznakami: a) slika razrezanega in označenega vzorca, ulitega v merilno celico Croning, b) slika razrezanega in označenega vzorca, ulitega v trajno stožčasto merilno celico iz sive litine

The cooling curves were obtained with a data acquisition during the cooling and solidification processes using a measuring card DAQ Pad-MI0-16XE-50 and the corresponding software LabView 7.0. The cooling curves were afterwards plotted and analyzed with the Origin 7.0 software, determining the reference temperatures of the phase transformation in real samples.

A simultaneous thermal analysis was performed with the differential scanning calorimetry (DSC) method on the NETZSCH equipment, type Jupiter 449C on sample 6P-1 using the heating and cooling techniques with the purpose of establishing the reference temperatures of phase transformations and solidification intervals, as well as the corresponding enthalpies and the specific heat extraction for each phase.

3 RESULTS AND DISCUSSION

The chemical composition of the investigated charge was determined with an optical emission spectrometer and it is presented in **Table 1**. The sample for the

Table 1: Chemical composition of the EN AW-AlMg4.5Mn0.7 alloy
Tabela 1: Kemijska sestava zlitine EN AW-AlMg4,5Mn0,7

Chemical composition in mass fractions, *w*/%									
Si	Fe	Cu	Mn	Mg	Cr	Zn	Ti	Be	Na
0.14	0.38	0.01	0.43	4.56	0.11	0.006	0.021	0.0057	0.0012

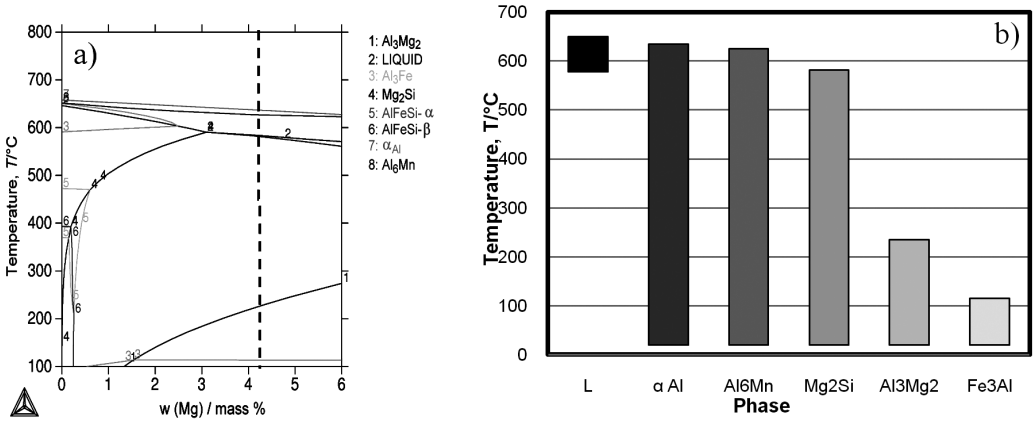

Figure 4: Thermodynamical calculation of the equilibrium-phase diagram of the investigated EN AW-AlMg4.5Mn0.7 alloy: a) polythermal section of the equilibrium-phase diagram, b) areas of temperature stability for particular phases
Slika 4: Ravnotežni termodinamski izračun faznega diagrama za zlitino EN AW AlMg4,5Mn0,7: a) izopletni ravnotežni fazni diagram, b) temperaturna območja stabilnosti posameznih faz

chemical analysis was taken out during the casting of an ingot with a length of about 0.5 m.

There were no significant deviations of the chemical composition from the referential values prescribed by the standard EN 573-3: 2002.[13]

The thermodynamical calculation of the particular phase stability, along with the initial temperature of 20 °C, the pressure of 10^5 MPa and the specific chemical composition of the examined alloys (4.56 % Mg, 0.43 % Mn, 0.38 % Fe and 0.14 % Si), resulted in an isoplete phase diagram (**Figure 4a**) and an area of the temperature stability of each phase (**Figure 4b**).

The equilibrium solidification of the EN AW-AlMg4.5Mn0.7 alloy proceeds as follows (**Figure 4**): primary crystals of α_{Al}, Al_6Mn and Mg_2Si. Under the solidus, the Al_3Mg_2 (in the literature known as Al_8Mg_5) and Al_3Fe phases also precipitated.

It was determined that at 635 °C the primary crystals of α_{Al} are the first to be evaluated, which corresponds to the liquidus temperature. Shortly after the evaluation of the α_{Al} crystals at 625 °C the first eutectic phase, Al_6Mn, was solidified due to a relatively high content of manganese in this alloy. The beginning of the secondary eutectic solidification ($Mg_2Si + \alpha_{Al}$) can be predicted to occur at 581 °C. From the diagram in **Figure 4a** the solidus temperature of 578 °C was determined, which is associated with the maximum contribution of primary dendrites of aluminum at this temperature. A precipitation of the first phase, Al_8Mg_5, starts at 235 °C in the solid state. This is followed by the precipitation of the iron phase, Al_3Fe, at 115 °C. An interpretation of these diagrams indicates a complex solidification sequence with a series of interconnected reactions. The melt is stable after the initial temperature of 650 °C to 578 °C.

On the basis of the data calculated by the Thermo-Calc 5.0 software (**Figure 4a**) and their stability histogram (**Figure 4b**), an evaluation sequence can be determined as shown in **Table 2**.

Table 2: Sequence of the microstructural-constituent evaluation made on the basis of the data calculated with the Thermo-Calc software
Tabela 2: Izračunane reakcije in razvoj mikrostrukturnih sestavin pri strjevanju zlitine z uporabo programa Thermo-Calc

Predicted reactions	Temperature, *T*/°C	
$L \rightarrow \alpha_{Al} + L'$	635	Liquidus temperature, T_L
$L' \rightarrow \alpha_{Al} + Al_6Mn + L''$	625	Primary eutectic temperature, T_{E1}
$L'' \rightarrow \alpha_{Al} + Mg_2Si$	581	Secondary eutectic temperature, T_{E2}
$\alpha_{Al} \rightarrow Al_8Mg_5 + \alpha_{Al}'$	235	Precipitation temperature of the low temperature phases
$\alpha_{Al}' \rightarrow Al_3Fe$	115	

where *L'* is melt composition *L'*; *L''* is melt composition *L''*.

The cooling curves of sample 6P-1 cast in a cone-shaped, grey iron-measuring cell are presented in **Figure 5**. The cooling curve of the sample from the cone vertex is called 6P-11, the one taken from the middle of the cone is 6P-12 and the one taken from the cone base is 6P-13.

The cooling curves in **Figure 5** indicate a significant mutual deviation from the values for reference temperatures of the phase changes, as well as of the curve

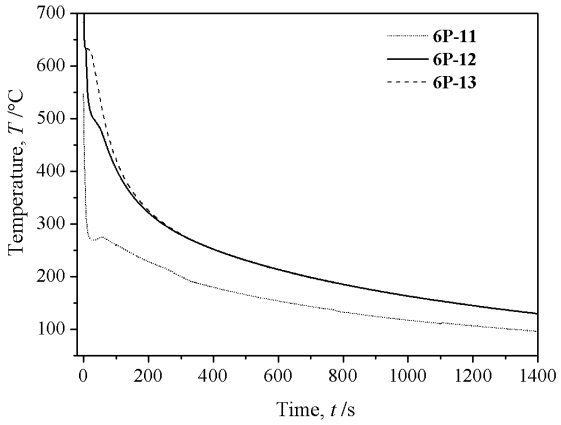

Figure 5: Cooling curves of sample 6P-1 cast in a cone-shaped, grey iron-measuring cell
Slika 5: Ohlajevalna krivulja vzorca 6P-1, ulitega v trajno stožčasto kokilo iz sive litine

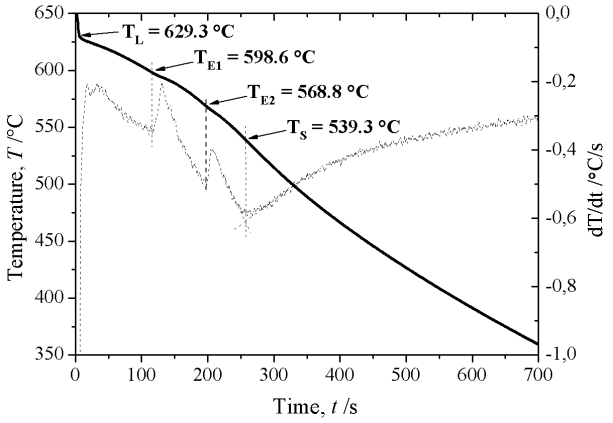

Figure 6: Cooling curve and differential cooling curve of sample 6P-1, STA of the EN AW-AlMg4.5Mn0.7 alloy cast in the measuring cell made with the Croning process
Slika 6: Ohlajevalna krivulja in odvod ohlajevalne krivulje vzorca 6P-1, STA zlitine EN AW-AlMg4,5Mn0,7, ulite v merilno celico Croning

gradient, indicating significant differences in the cooling rates. The cooling rates of each sample were established from the cooling curves, where the temperature and the time intervals were determined from the difference between the maximum detected temperature (the pouring temperature) and the nucleation temperature established on the first derivative curve.

The curve of sample 6P-13 features the least variation in temperature values, and with its smallest gradient it also has the lowest cooling rate of r_c = 10.8 °C/s. Using the first and the second derivation cooling curves, the liquidus temperature T_L = 632.7 °C, the temperatures of the first and the second eutectics T_{E1} = 607.6 °C and T_{E2} = 570.9 °C, as well as the solidus temperature T_S = 540.9 °C were determined. The solidification time for the cooling rate of sample 6P-13, as the difference of the times, at which the liquidus and solidus temperatures occur, amounts to Δt_s = 65 s.

The cooling curve of sample 6P-12 indicates the cooling rate of r_c = 40.3 °C/s, and here the following temperatures of the phase transitions were obtained: T_L = 634.0 °C, T_{E1} = 594.0 °C, T_{E2} = 544.0 °C and T_S = 523.7 °C. There is a marked fall in all the temperatures compared to the previous cooling rate of 10.8 °C/s, except for T_L whose deviation is minimum and amounts to ≈1.3 °C. In this case the solidification is completed in Δt_s = 11.2 s.

The curve of sample 6P-11 shows the cooling rate of r_c = 124.0 °C/s that makes the oscillations more pronounced, and there is an uncertainty in determining the appropriate, respective phase-transition temperatures.

Figure 6 shows a typical cooling curve and its first derivation of the tested sample 6P-1, STA, cast in the measuring cell made with the Croning process. On the cooling curve of the tested sample 6P-1, STA (**Figure 6**), there are no pronounced peaks due to a relatively low cooling rate in the measuring cell made with the Croning process of only 8.3 °C/s. By means of the first derivation of the cooling curve, the liquidus and solidus temperatures can be determined, as well as the eutectic temperatures of the tested sample.

From the cooling curve of sample 6P-1, STA, it could be noted that the solidification starts at the temperature of T_L = 629.3 °C. The eutectic solidification of the melt into eutectic E1 occurs at the temperature of T_{E1} = 598.6 °C. At T_{E2} = 568.8 °C the second eutectic E2 occurs. The solidification of sample 6P-1, STA, ceases at the temperature solidus of T_S = 539.3 °C, so that the obtained time of the solidification amounts to Δt_s = 250.1 s.

The reference temperatures of the phase transformations of the samples tested with a DSC analysis (6P-1, DSC) in the measuring cell made with the Croning process (6P-1, STA), and for individual places in the

Table 3: Reference temperatures of the phase changes at different cooling rates for sample 6P-1 of the EN AW-AlMg4.5Mn0.7 alloy
Tabela 3: Značilne temperature faznih premen pri različnih ohlajevalnih hitrostih za vzorec 6P-1 zlitine EN AW-AlMg4,5Mn0,7

Cooling curve/ Sample indication	r_c/(°C/s)	T_L/°C	T_{E1}/°C	T_{E2}/°C	T_S/°C	Δt_s/s
TCW	0	635.0	625.0	581.0	578.0	–
6P-1, DSC	0.17	637.2	595.8	569.6	527.0	660.6
6P-1, STA	8.3	630.8	598.5	568.3	538.9	250.1
6P-13	10.8	632.7	607.6	570.9	540.9	65.0
6P-12	40.3	634.0	594.0	544.0	523.7	11.2

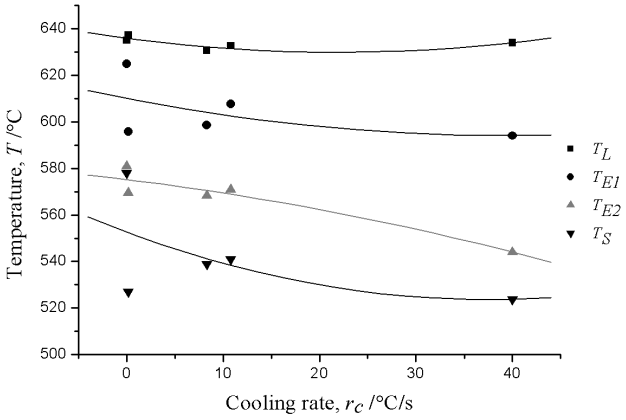

Figure 7: Dependences of the reference temperatures of the phase changes on the cooling rates of the EN AW-AlMg4.5Mn0.7 alloy samples

Slika 7: Karakteristične temperature faznih premen zlitine EN AW-AlMg4,5Mn0,7 v odvisnosti od ohlajevalne hitrosti

cone-shaped die cast (6P-13 and 6P-12), following the ascending cooling rate, are presented in **Table 3**.

The physical models for the dependences of particular reference temperatures of the phase transformations on the cooling rates were made. Exponential types for T_L, T_{E1}, T_{E2} and T_S are graphically presented in **Figure 7**.

The liquidus temperature, $T_{L,}$ is cooling-rate dependent and it covers the range of 6.4 °C. The evaluation of the primary eutectic phase E_1 occurs in the temperature interval from 625.0 °C, for the equilibrium solidification, to 594.0 °C, for the cooling rate of r_c = 40.3 °C/s, and with a tendency of the temperature T_{E1} decrease. The T_{E2} curve has a similar trend. The largest decrease in the solidus temperature T_S was observed at the highest cooling rate. The decrease was 54.3 °C of the cooling rate at the equilibrium solidification (r_c = 0 °C/s) to the maximum measured cooling rate of the sample from the middle part of the cone-shaped mould (r_c = 40.3 °C/s). The deviation in T_S from the equilibrium solidification (r_c = 0 °C/s) T_S = 578.0 °C to the cooling rate of r_c = 0.17 °C/s (sample 6P-1, DSC, T_S = 527.0 °C/s, is the result of the formation of eutectics, **Figure 7** and **Table 3**. Generally speaking, the liquidus temperature T_L remains almost unchanged, while the temperatures T_{E1}, T_{E2} and T_S decrease with an increase in the cooling rate.

The physical models for the dependences of liquidus, primary and secondary eutectic temperatures and solidus temperature were illustrated with the following equations and the corresponding correlation coefficient R^2:

$$T_L = 636.00 - 0.55 \cdot r_c + 0.013 \cdot r_c^2 \qquad R^2 = 0.73 \qquad (1)$$

$$T_{E1} = 610.10 - 0.80 \cdot r_c + 0.010 \cdot r_c^2 \qquad R^2 = 0.26 \qquad (2)$$

$$T_{E2} = 575.19 - 0.51 \cdot r_c + 0.007 \cdot r_c^2 \qquad R^2 = 0.90 \qquad (3)$$

$$T_S = 552.67 - 1.54 \cdot r_c + 0.021 \cdot r_c^2 \qquad R^2 = 0.31 \qquad (4)$$

The largest deviations from the obtained function curves show the temperature of the first eutectic and solidus temperatures that also have the minimum correlation coefficient R^2.

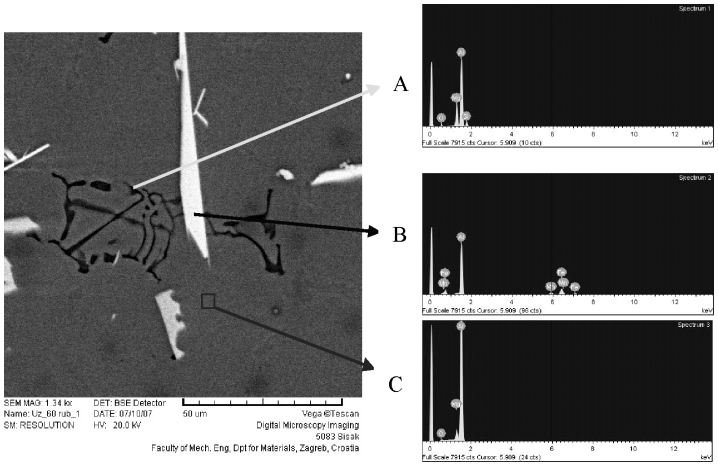

Place	Mg		Al		Si		Mn		Fe		O	
	w/%	*x*/%	*w*/%	*x*/%	*w*/%	*x*/%	*w*/%	*x*/%	*w*/%	*x*/%	*w*/%	*x*/%
A	16.36	16.99	67.61	63.27	8.18	7.35	–	–	–	–	7.85	12.38
B	–	–	65.41	79.60	–	–	6.56	3.92	28.03	16.48		
C	4.35	4.69	92.12	89.52	–	–	–	–	–	–	3.54	5.79

Figure 8: Microstructure of sample 6P-1 obtained with a scanning electron microscope (SEM) with the marked places of quantitative analysis performed by EDS, their particular spectrums and the quantitative-analysis results (place A – black phase: Mg, Si; stoichiometry Mg_2Si; place B – white phase: Al, Fe, Mn; stoichiometry $Al_6(Fe, Mn)$; place C – matrix: α_{Al}); w/% mass fraction; x/% mole fraction

Slika 8: Mikrostruktura vzorca 6P-1, posneta z vrstičnim elektronskim mikroskopom (SEM), z označenimi mesti kvantitativne analize (EDS) ter pripadajoči spektri in rezultati kvantitativne analize (mesto A – črna faza: Mg, Si; stehiometrija Mg_2Si; mesto B – bela faza: Al, Fe, Mn; stehiometrija $Al_6(Fe, Mn)$; mesto C – matrica: α_{Al}); w/% masni delež; x/% molski delež

The qualitative analysis of the microstructural constituents of the EN AW-AlMg4.5Mn0.7 alloy was performed in order to determine and/or confirm the presumed stoichiometry with the energy dispersive spectrometry (EDS) for all the investigated cooling rates. An example of the quantitative phase analysis of the as-cast sample 6P-1 is shown in **Figure 8**.

The analysis of sample 6P-1 (**Figure 8**) confirms the presence of the phase based on magnesium and silicon, which corresponds to the stoichiometric Mg_2Si phase, defined as the second eutectic phase ($\alpha_{Al} + Mg_2Si$) by the Thermo-Calc. The Mg_2Si phase is shown in the images as a black, irregular, branched-shaped phase (**Figure 8**, place A).

The phase based on manganese (Al_6Mn) was not established although its presence as the primary eutectic phase was assumed during the thermodynamic modeling of the solidification (TCW 5.0). However, the phases containing aluminum, manganese and iron were determined and they seem to correspond to the $Al_6(Fe, Mn)$ phases. These are the white phases in the structure that appear in various forms, such as needles (**Figure 8**, place B), the forms with a Chinese-script morphology (**Figure 9**) determined with a mapping analysis, or irregular rounded shapes. From the obtained results it could be concluded that, due to the non-equilibrium solidification, the above-mentioned primary eutectic ($\alpha_{Al} + Al_6Mn$) corresponded to eutectic ($\alpha_{Al} + Al_6(Fe, Mn)$).

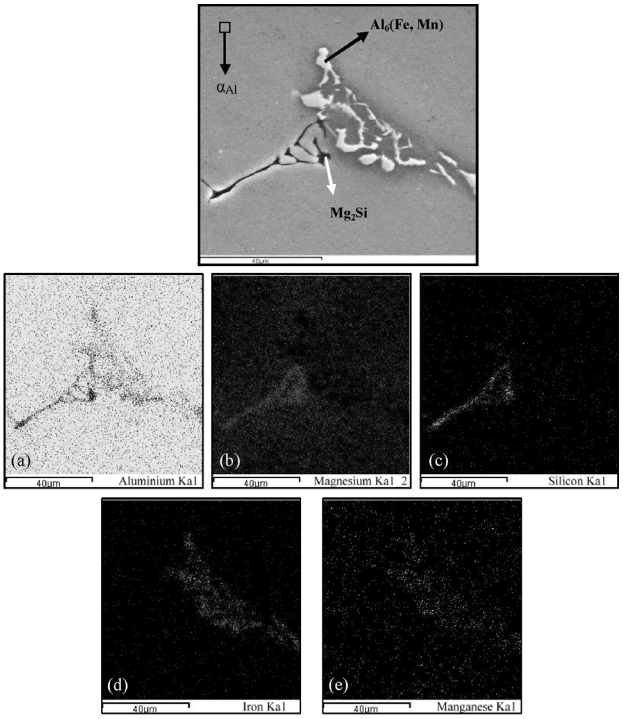

Figure 9: Microstructure (SEM) of sample 6P-1 obtained with the mapping analysis

Slika 9: Mikrostruktura (SEM) vzorca 6P-1 s ploskovno porazdelitvijo elementov v mikrostrukturi

Figure 9 shows that iron and magnesium are concentrated in the eutectic interdentritic regions. The concentration of magnesium was markedly elevated in the eutectic area, where silicon is also found, which indicates the occurrence of eutectic ($\alpha_{Al} + Mg_2Si$), **Figure 9b** and **9c**. In the areas with elevated concentrations of iron the elevated content of manganese is also observed, which confirms the existence of the first eutectic ($\alpha_{Al} + Al_6(Fe, Mn)$). The metal base containing aluminum and magnesium can be seen as the grey background (**Figure 8**, place C, **Figure 9**), where all of the above-mentioned phases are different.

These results were confirmed by the mapping and EDS analyses, **Figure 9**.

The presence of phases Al_8Mg_5 and Al_3Fe, which should be separated in the solid state, was not established although their presence was assumed during the thermodynamic modeling of solidification. This is attributed to the cooling conditions that are different from those assumed for the equilibrium conditions of solidification.

In addition to the above-mentioned phases present in sample 6P-1, the shrinkage porosity also appears in a small quantity. It appears in black color and with an irregular shape, formed in the dendritic mushy zones, where feeding is not possible, as shown in **Figure 10**.

By conducting a qualitative analysis of the microstructural constituents of samples 6P-1, DSC; 6P-1, STA; 6P-13, 6P-12 and 6P-11, the presence of equal intermetallic phases and porosity was also established for sample 6P-1.

Different cooling rates contribute to the development of microstructural constituents with different sizes and morphologies. It is well known that a high cooling rate prompts the refining effect because there is not enough time available for achieving the full size as in the cases of low cooling rates. **Figure 10** shows a comparative number of images of the microstructures of samples 6P-1, DSC; 6P-1, JTA, 6P-13, 6P and 6P-12-11, cast at different cooling rates and recorded with a scanning electron microscope with different magnifications, which are listed on each figure.

When examining **Figure 10** in terms of a uniform magnification, the differences in the sizes and the morphologies of the microstructural constituents of individual samples are not revealed; the intermetallic phases are evenly distributed and have the same morphology.

However, a comparison of the metallographic images of different samples with a scanning electron microscope with the same magnification shows a significant variation in the sizes of the surveyed intermetallic phases and pores. The particles of the intermetallic phase ($Al_6(Fe, Mn)$) and Mg_2Si formed at the slowest cooling rate (r_c = 0.17 °C/s), **Figure 10a**, are visible and distinguishable to the naked eye, and are the largest in comparison with the ones occurring at the other cooling rates. As the cooling rate grows these intermetallic

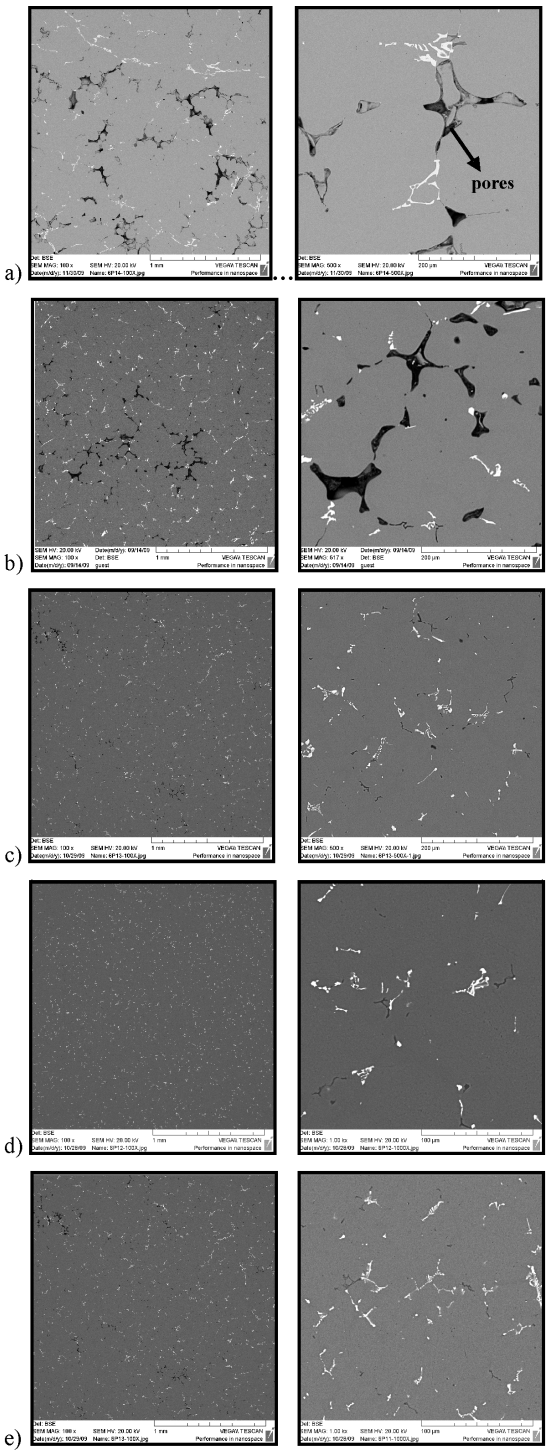

Figure 10: Microstructures (SEM) of EN AW-AlMg4.5Mn0.7 samples according to the increasing cooling rates, etched with 0.5 % HF: a) sample 6P-1, DSC, at r_c = 0.17 °C/s, b) sample 6P-1, STA, at r_c = 8.3 °C/s, c) sample 6P-13 cast into a cone-shaped measuring cell at r_c = 10.8 °C/s, d) sample 6P-12 cast into a cone-shaped measuring cell at r_c = 40.3 °C/s, e) sample 6P-11 cast into a cone-shaped measuring cell at r_c = 124.0 °C/s

Slika 10: Mikrostrukture (SEM) zlitine EN AW-AlMg4,5Mn0,7 v odvisnosti od ohlajevalne hitrosti, jedkane z 0,5 % HF: a) vzorec 6P-1, DSC z r_c = 0,17 °C/s, b) vzorec 6P-1, STA z r_c = 8,3 °C/s, c) vzorec 6P-13, ulit v trajno kokilo z r_c = 10,8 °C/s, d) vzorec 6P-12, ulit v trajno kokilo z r_c = 40,3 °C/s, e) vzorec 6P-11, ulit v trajno kokilo z r_c = 124,0 °C/s

phases become finer and indistinguishable at low magnifications, **Figure 10e**.

The greatest reduction in the particle size of both intermetallic phases (Al_6(Fe, Mn), Mg_2Si) is noted after an increase in the cooling rate of r_c = 0.17–10.8 °C/s (**Figures 10a** and **10b**), followed by a less intense decrease in the cooling rate of r_c = 124.0 °C/s (**Figure 10e**).

Using a visual method, it is difficult to conclude how the proportion of the total surface of the intermetallic phases Al_6(Fe, Mn) and Mg_2Si change with the change in the cooling rate. It is necessary to conduct a detailed quantitative analysis.

At the low cooling rates, the pores in the microstructure are most visible as larger dark areas, **Figures 10a** and **10b**.

The largest particles have pores in the sample after the differential scanning calorimetry (6P-1, DSC), when the lowest cooling rate of r_c = 0.17 °C/s is achieved and there is no directional solidification. The reduction of the size of the porosity and their total share in the microstructure following an increase in the cooling rate can be seen, especially with the cooling rate increase from r_c = 0.17–8.3 °C/s, followed by a significantly smaller decrease. Even at higher magnifications, these pores are almost unnoticeable to the naked eye at the highest cooling rates (r_c = 40.3 °C/s and 124.0 °C/s), **Figures 10d** and **10e**.

The reason for this is the fact that an increase in the cooling rate causes an increase in the degree of undercooling, which is then also reflected in an increase in the nucleation potential.

When examining **Figure 10** the presence of the other intermetallic phases was not noticed, as confirmed with the EDS analysis.

4 CONCLUSIONS

The influence of different cooling rates on the reference temperatures of the phase transformations during the solidification of the EN AW-AlMg4.5Mn0.7 alloy was examined. The following conclusions can be made:

- A microstructural analysis, performed with the electron microscopes resulted in a recognition of particular microstructural constituents of the EN AW-AlMg4.5Mn0.7 alloy: primary crystals of α_{Al}, Al_6(Fe, Mn) (white phase) and Mg_2Si (black phase). The presence of phases Al_8Mg_5 and Al_3Fe was not established due to the deviations of the equilibrium cooling and solidification conditions. These results were confirmed with the mapping and EDS analyses. In addition to the above-mentioned phases, the porosity also appeared; the pores are black and irregularly shaped.
- By using a simple thermal analysis of sample 6P-1 of the EN AW-AlMg4.5Mn0.7 alloy at different cooling rates and solidification conditions (cast into a

measuring cell made with the Croning process and a permanent cone-shaped measuring cell), together with differential scanning calorimetry, the cooling rates of r_c = (0.17; 8.3; 10.8; 40.3 and 124.0) °C/s were obtained. The following reference temperatures from the solidification were determined: T_L, T_{E1}, T_{E2}, T_S and Δt_s. Mathematical models were calculated for the dependence of the reference temperatures on the cooling rates (equitation (1)–(4)). Generally speaking, liquidus temperature T_L remains almost unchanged, while temperatures T_{E1}, T_{E2} and T_S decrease with an increase in the cooling rate.

- By examining the samples at the same magnification, the differences in the size and the morphology of individual microstructural constituents of each sample are not revealed; the intermetallic phases are evenly distributed and have the same morphology.
- Using a visual method to observe images with the SEM, it was found that an increase in the cooling rate leads to a decrease in the particle size of both intermetallic phases $Al_6(Fe, Mn)$ and Mg_2Si, and that subsequently leads to a refining of the microstructure. It was also found that the pores are the largest at the slowest cooling rate (r_c = 0.17 °C/s), while an increase in the cooling rate leads to a reduction of the pores' size, as well as to a reduction of their total share in the microstructure.

Acknowledgements

The research was performed in the frame of the national project 124-0000000-1503 financed by the Ministry of Science, Education and Sports of Croatia.

5 REFERENCES

[1] Z. Zhu, Ageing and strengthening of cold-rolled Al-Mg(-Cu)-Si-Mn alloys: experimental analysis and modeling, Ph.D. Thesis, University of Southampton, Faculty of Engineering, Science & Mathematics, Southampton, United Kingdom 2006

[2] I. J. Polmear, Light Alloys, Metallurgy of the light metals, Arnold, London 1995

[3] S. Lathabai, P. G. Lloyd, The effect of scandium on the microstructure, mechanical properties and weldability of a cast Al-Mg alloy, Acta Materialia, 50 (**2002**), 4275–4292

[4] ASM Specialty Handbook®, Aluminum and Aluminum Alloys, ASM International, Materials Park, Ohio 2002

[5] T. Aiura, N. Sugawara, Y. Miura, The effect of scandium on the as-homogenized microstructure of 5083 alloy for extrusion, Materials Science and Engineering, A280 (**2000**), 139–145

[6] D. G. Eskin, Physical metallurgy of Direct Chill casting of aluminium alloys, CRC Press/Taylor and Francis Group, Boca Raton 2008

[7] L. F. Mondolfo, Aluminum alloys, structure and properties, Butterworths, London 1976

[8] ASM Handbook®, Vol. 3, Alloy phase diagrams, ASM International, Materials Park, Ohio 1992

[9] J. L. Murray, Al-Mg (Aluminium-Magnesium), Binary systems of aluminium – admixture and their importance for metallurgy, Vysoká škola báňská-Technická Univerzita, Ostrava 2003

[10] M. M. R. Jaradeh, Ph. D. Thesis, The effect of processing parameters and alloy composition on the microstructure formation and quality of DC cast aluminium alloys, Mid Sweden University, Sundsvall, Sweden 2006

[11] A. Chaijaruwanich, P. D. Lee, R. J. Dashwood, Y. M. Youssef, H. Nagaumi, Evolution of pore morphology and distribution during the homogenization of Direct Chill cast Al-Mg alloys, Acta Materialia, 55 (**2007**), 285–293

[12] P. D. Lee, R. C. Atwood, R. J. Dashwood, H. Nagaumi, Modeling of porosity formation in Direct Chill cast aluminum-magnesium alloys, Materials Science and Engineering A, 328 (**2002**), 213–222

[13] EN 573-3: 2002, Aluminium and aluminium alloys – chemical composition and form of wrought products – Part 3: Chemical Composition, European Committee for Standardization (CEN), Brussels 2002

[14] N. Dolić, Ph.D. Thesis, Influence of solidification and cooling condition on the properties of semicontinuous cast slabs of Al-Mg alloy, University of Zagreb, Faculty of Metallurgy, Sisak, Croatia 2010